

Microbial Communities Collectively Recycle Cadavers Over One Year of Human Decomposition

Allison R. Mason¹, Lois S. Taylor², Naomi E. Gilbert¹,
Steven W. Wilhelm¹, Jennifer M. DeBruyn^{1,2*}

¹Department of Microbiology, University of Tennessee-Knoxville, 1311
Cumberland Avenue, Knoxville, 37996.

²Department of Biosystems Engineering and Soil Science, University of
Tennessee-Knoxville, 2506 E.J. Chapman Drive, Knoxville, 37996.

*Corresponding author(s). E-mail(s): jdebruyn@utk.edu;

Abstract

During terrestrial vertebrate decomposition, host and environmental microbial communities work together to drive biogeochemical cycling of carbon and nutrients. These mixed communities undergo dramatic restructuring in the resulting decomposition hotspots. To reveal the succession of both the active microbial members and the metabolic pathways they use, we generated metatranscriptomes from soil samples collected over one year from below three decomposing human bodies. Soil microbes increased expression of heat shock proteins in response to decomposition products changing physiochemical conditions (*i.e.*, reduced oxygen, high salt). Increased fungal lipase expression implicated fungi as key decomposers of fat tissue. Expression of nitrogen cycling genes was phased with soil oxygen concentrations: during hypoxic soil conditions, genes catalyzing N-reducing processes (*e.g.*, hydroxylamine to nitric oxide and nitrous oxide to nitrogen gas during reduced oxygen conditions) were increased, followed by increased expression of nitrification genes once oxygen diffused back into the soil. Increased expression of bile salt hydrolases implicated a microbial source for

the high concentrations of taurine typically observed during vertebrate decomposition. Collectively, microbial gene expression profiles remained altered even after one year. Together, we show how human decomposition alters soil microbial gene expression, revealing both ephemeral and lasting effects on soil microbial communities.

Keywords: Human Decomposition, Microbial Succession, Metatranscriptomics, Soil Microbial Ecology

Introduction

Soil microbial communities are important drivers of ecosystem processes in terrestrial environments. Many soil microbes are decomposers that degrade complex organic matter and drive nutrient cycling in terrestrial ecosystems. Environmental disturbances can impact the presence and/or activity of soil microorganisms involved in these cycles, ultimately affecting nutrient availability and greenhouse gas emissions, such as CO₂ and N₂O [1, 2]. Vertebrate death and subsequent carcass deposition in terrestrial ecosystems is one disturbance resulting in the deposition of large quantities of organic C and N [3–10], along with other elements (P, K, S, *etc.*) [11], which collectively stimulate microbially-mediated biogeochemical cycling. In addition to this, changes in pH, temperature, and fluctuations in soil oxygen provide abiotic filtering further impacting microbial metabolic strategies [7–9, 11–13]. Vertebrate decomposition also results in mixing of host and environmental microbes: the animal’s microflora are flushed into the soil along with decomposition products where they further contribute to decomposition processes (*e.g.*, organic nitrogen mineralization) [14].

While C and N transformations have been documented during decomposition, the functional response of microbes and their roles in nutrient cycles remain unclear. The composition and structure of decomposition-impacted soil microbial communities have been investigated using sequencing of marker genes amplicons (*i.e.*, 16S rRNA, 18S

rRNA, ITS). This has allowed for the identification of changes in microbial biodiversity and taxonomic succession in response to vertebrate decomposition, revealing patterns that include increases in the anaerobic taxa *Firmicutes* and *Bacteroidetes* [15]. However, few studies have integrated soil biogeochemistry with microbial community composition, which can further help to describe microbial ecology in these decomposition systems. Taylor et al. (2024) [13] showed that fungal community shifts were linked to changes in soil dissolved oxygen, highlighting interactions between soil microbes and changes in the surrounding environment. While insightful for making potential connections between taxa and environment, these analyses do not inform which taxa are active members of the community, which functional pathways/genes are expressed, and how these pathways facilitate decomposition processes.

RNA sequencing (*i.e.*, metatranscriptomics) and metabolomics can be used to investigate microbial community functional succession during decomposition. They can identify how ecological functions, including C and N cycling, are impacted by decomposition events in terrestrial ecosystems. To date, applications of metatranscriptomics to vertebrate decomposition samples have been limited to internal host communities [16, 17]: Burcham et al. (2019) [16] revealed differential expression of amino acid and carbohydrate metabolism in the heart during mouse decomposition, while Ashe et al. (2021) [17] documented taxonomic shifts in gene expression of oral microbial communities during human decomposition.

We expected that the impacted soil microbial community, which includes a mix of host and environmental taxa, would also have altered gene expression profiles, given the release of decomposition byproducts into the soil during terrestrial decomposition. We previously assessed the decomposition-impacted soil metabolome [18], demonstrating a prevalence of amino acids and suggesting upregulation of organic nitrogen metabolic pathways. Additionally, DeBruyn et al. (2021) [18] showed the soil metabolome was

139 surprisingly still altered compared to starting conditions at the end of that 21-week
 140 study, suggesting long-term impacts of decomposition on soil microbial functioning.
 141
 142 Here, we investigated soil microbial gene expression during a one-year period of human
 143 decomposition. The overarching goal of this work was to assess the effects of vertebrate
 144 decomposition on ecosystem function by characterizing community-level shifts in soil
 145 microbial function. We hypothesized that: (i) gene expression would shift over time as
 146 resources were consumed and transformed and soil chemical and physical conditions
 147 changed due to the influx of decomposition products during soft tissue degradation
 148 [8, 9, 18]; (ii) gene expression for enzymes involved in nitrogen cycling would be altered,
 149 as changes in nitrogen pools have been previously described in decomposition soils [8];
 150 (iii) expression of genes involved in lipid metabolism would increase, as lipids from
 151 the body entered the soil during decomposition and previous studies identified lipoly-
 152 tic organisms in decomposition soils [12, 19]; (iv) microbial expression profiles in the
 153 impacted soil would not fully recover and remain altered even after a year, as previ-
 154 ous studies have shown that community composition was still altered at least a year
 155 after decomposition began [20, 21]. We analyzed metatranscriptomes of soil samples
 156 collected at six key timepoints over one year of human decomposition to determine
 157 the identity of active populations and the expression of genes and pathways relevant
 158 to the enhanced biogeochemical cycling observed in decomposition hotspots. We com-
 159 pared gene expression between decomposition timepoints and control soils that were
 160 unexposed to decomposition products to identify functions or functional pathways
 161 of interest. We show: (i) decomposition shifts soil microbial community gene expres-
 162 sion, with the effects still measurable after one year; (ii) expression of genes related to
 163 stress response are elevated in decomposition soils; (iii) expression of genes encoding
 164 triacylglycerol lipase differed between fungi (increased) and bacteria (decreased), indi-
 165 cating differential responses between bacterial and fungal decomposers; (iv) evidence
 166 for phased nitrification and denitrification, driven by changes in soil dissolved oxygen;
 167
 168
 169
 170
 171
 172
 173
 174
 175
 176
 177
 178
 179
 180
 181
 182
 183
 184

(v) evidence for organic sulfur processing (taurine) via bile salt hydrolases. This direct assessment of function expands the fundamental understanding of terrestrial vertebrate decomposition, providing insight into pathways of biogeochemical cycling within these hotspots.

Results

Soil Physiochemistry

Soil chemistry was altered in response to the presence of decomposing human cadavers, with multiple parameters still impacted after one year [13]. Generally, soil pH decreased and remained low in decomposition soils. Soil electrical conductivity (EC) increased in response to decomposition, remaining elevated through approximately day 58 before gradually decreasing throughout the remainder of the study (Supplementary Fig. 1). Respiration (evolved CO₂) increased by an order of magnitude beginning at day 12, which corresponded to a reduction in soil dissolved oxygen (DO) to 29% - 48.9%. Ammonium concentrations increased 78-fold, reaching maximum concentrations between days 12 and 58. This was followed by decreased ammonium and increased nitrate concentrations at day 86, with nitrate concentrations reaching a maximum at day 168 (Supplementary Fig. 1).

Microbial gene expression in response to human decomposition

Gene expression profiles in decomposition-impacted soils shifted away from controls and day zero samples as decomposition progressed (Fig 1A). Expression was most different from controls on study days 58, 86, 168 (Supplementary Fig. 2), before starting to return toward control conditions on study day 376. After one year of decomposition, soil gene expression profiles had not returned to pre-decomposition conditions, as evidenced by their clustering away from controls and day zero samples in the MDS plot (Fig 1A).

231 Some correlations were observed between gene expression shifts and soil physiochemi-
 232 cal data at decomposition timepoints. Canonical correspondence analysis (CCA) was
 233 used to constrain gene expression data with soil physiochemical data (Fig 1B). CCA1
 234 and CCA2 explained 29.2% and 18.1% of the variance in gene expression, respectively.
 235 Transcript profiles at day 12 were associated with an increase in soil carbon to nitrogen
 236 ratio (C:N). Gene expression profiles at days 58 to 86 were positively correlated with
 237 increased soil temperature, EC, and evolved CO₂, while study day 168 was associated
 238 with elevated levels of soil NO₃. Further, Permutational Analysis of Variance (PER-
 239 MANOVA) revealed that internal accumulated degree hours (ADH) ($p = 0.001$), soil
 240 temperature ($p = 0.039$), pH ($p = 0.033$), and EC ($p = 0.031$) significantly explained
 241 some of the variation in gene expression profiles ($p < 0.05$). No other soil chemical
 242 variables were significant at $\alpha = 0.05$ (Supplementary Table 1).
 243
 244 Overall, decomposition changed soil gene expression profiles over the one-year study
 245 relative to control soils. Differential expression analysis between decomposition and
 246 control soils identified 7,047 down-regulated and 38,425 up-regulated genes. Gene
 247 transcripts that were associated with control soils belonged to a wide variety of clus-
 248 ters of orthologous genes (COG) functional categories. Specifically, the top 20 genes
 249 whose expression was higher in control soils belonged to ten unique COG categories,
 250 including signal transduction mechanisms, transcription, and those of unknown func-
 251 tion. In contrast, the top 20 genes whose expression was higher in decomposition soils
 252 only fell into four COG categories (Supplementary Fig. 3 A): 1) post-translational
 253 modification, protein turnover, and chaperones; 2) energy production and conversion;
 254 3) cell motility; and 4) carbohydrate transport and metabolism. The most common
 255 COG category represented in decomposition soils (80% of the top 20 genes) was post-
 256 translational modification, protein turnover, and chaperones. Within this category,
 257 several heat shock stress response genes were identified, including clpB, dnaK, groL2,
 258 SSA2, HSP82, and clpB (Supplementary Table 2). Further investigation of these genes
 259
 260
 261
 262
 263
 264
 265
 266
 267
 268
 269
 270
 271
 272
 273
 274
 275
 276

over time shows that their expression increased, typically reaching maximum transcript levels around study days 58 and 86 (Fig 2). This corresponded to elevated soil temperatures below decomposing bodies between study days 12-80, with soil temperatures increasing to approximately 43°C [13], as well as maximum soil EC and minimum dissolved oxygen measurements between days 12 and 58 (Supplementary Fig. 1).

Taxonomy associated with top differentially expressed gene transcripts also differed between control and decomposition soils. The top 40 most significant differentially expressed gene transcripts in decomposition soils were associated with Fungi, *Actinobacteria*, and *Xanthomonadales*, while gene transcripts in controls were associated with *Acidobacteria*, *Cyanobacteria*, *Proteobacteria* (α , δ , γ), and *Planctomycetes* (Supplementary Fig. 3 B). The greatest number of differentially expressed genes relative to control samples was observed at day 86, where we saw 145,460 and 124,883 up- and down-regulated genes, respectively.

Temporal gene expression shows shifted decomposer functions

Differential expression analysis between sequential study days revealed which genes were altered during decomposition. The top ten transcripts that changed in representation (increased/decreased), determined by the lowest p-values from differential expression analysis, are reported in Supplementary Table 3 and Fig 3.

Expression of genes annotated with the COG categories cell wall/membrane/envelope biogenesis, inorganic ion transport and metabolism, and carbohydrate transport and metabolism increased proportionally from day 0 to 12. In contrast, expression of secondary metabolite biosynthesis, transport, and catabolism genes decreased during this period (Fig 3A). Transcripts from *Bacilli* and *Clostridia* increased, while transcripts from *Actinobacteria* decreased between study days zero and 12 (Fig 3).

323 Between days 12 and 58, 90% of the top 10 upregulated genes were associated with
 324 the translation, ribosomal structure and biogenesis COG and all were taxonomically
 325 associated with *Betaproteobacteria* (Fig 3A,B). Many of these genes were annotated
 326 as ribosomal protein large (RPL), involved in ribosomal binding. Genes across multi-
 327 ple COG categories with taxonomic associations to *Bacilli* and *Clostridia* decreased
 328 between study days 12 and 58, six of which were transcripts that previously increased
 329 between days zero and 12 (Fig 3B, Supplementary Table 3).
 330
 331 Multiple transcripts associated with the energy production and conversion COG, as
 332 well as transcripts annotated as inorganic transport and metabolism, and translation,
 333 ribosomal structure and biogenesis, increased between days 58 and 86 (Fig 3A). Two of
 334 the upregulated energy and production and conservation transcripts were associated
 335 with cytochrome c oxidase subunits in *Betaproteobacteria*, while another was anno-
 336 tated as *hao*, encoding the enzyme hydroxylamine dehydrogenase which is involved in
 337 conversion of hydroxylamine to nitrite during nitrification (Supplementary Table 3).
 338 Further investigation into hydroxylamine dehydrogenase showed a significant increase
 339 in *hao* transcripts at day 86 followed by subsequent decreases at days 168 and 376
 340 ($F = 4.183$; $p = 0.02$). This increase corresponded to decreased soil ammonium lev-
 341 els and subsequent accumulation of nitrate (Supplementary Fig. 1). Half of the 10
 342 most downregulated genes between days 58 and 86 were not assigned to a COG (*i.e.*,
 343 unclassified) or were of unknown function.
 344
 345 Differential expression comparing study days 86 with 168 and 168 with 376 identified
 346 genes across a variety of functional categories, with many unclassified in the COG
 347 database or with unknown function (Fig 3A). Expression of carbohydrate transport
 348 and metabolism genes associated with *Bacilli* decreased between day 168 and 376.
 349 *Acidobacteria* transcripts increased in decomposition-impacted soils between study
 350 day 168 and 376, but were not associated with any single COG category (Fig 3B).
 351
 352
 353
 354
 355
 356
 357
 358
 359
 360
 361
 362
 363
 364
 365
 366
 367
 368

Organic carbon metabolism

We expected to observe increased expression of lipid metabolizing genes during active and advanced decomposition as microbes degraded lipids deposited in the soil [19]. Therefore, we investigated changes in triacylglycerol lipase (enzyme commission number: 3.1.1.3) gene transcription in our soils. Generally, lipase transcripts decreased as decomposition progressed (HLM $F = 6.564$, $p < 0.001$), however we also observed a significant interaction between study day and taxonomic annotation ($F = 8.786$; $p < 0.001$). Specifically, lipase gene transcripts annotated as bacteria decreased with decomposition time ($F = 10.392$; $p = 0.001$), while fungal lipase transcripts increased, reaching a maximum at study day 58 ($F = 4.509$; $p = 0.015$) (Fig 4).

Nitrogen- and sulfur compound transformations

Expression of nitrogen cycling genes was impacted in response to human decomposition. Due to the detection of hydroxylamine oxidoreductase (*hao*) transcripts in our differential expression analysis, and our hypotheses predicting changes to nitrogen transformation processes, the expression of genes encoding common enzymes involved in nitrogen cycling (*nifH*, *nirB*, *nirK*, *norB*, *nosZ*, *nrfA*, *nxrA*, and *amoA*) were assessed using their enzyme commission numbers (Fig 5A,B). *nifH*, encoding a subunit of nitrogenase which is involved in nitrogen fixation, displayed little to no changes in gene expression between control and decomposition soils. Transcripts for two genes encoding enzymes contributing to the last two steps of denitrification, *norB* (nitric oxide reductase) and *nosZ* (nitrous oxide reductase), increased between study days 12 and 86, and decreased at study day 168 before increasing again at day 376. In contrast, expression of genes encoding nitrate reductase, *narG*, and NO-forming nitrite reductase, *nirK*, remained low until day 376 when transcripts for both genes increased. As noted above, expression of *hao*, encoding hydroxylamine dehydrogenase, increased at study day 86 before decreasing at remaining timepoints (Fig 3A, Fig 5B). Expression

415 of *amoA*, encoding a subunit of ammonia monooxygenase, and *nxrA*, encoding a sub-
416 unit of nitrite oxidoreductase, which are involved in nitrification, changed in response
417 to decomposition. *amoA* transcripts initially decreased at day 12, remaining reduced
418 until study day 376. Similarly, abundance of transcripts encoding enzymes involved
419 in dissimilatory nitrate reduction, *nirB*, and *nrfA*, was low for the first 168 days, with
420 *nrfA* expression increasing at day 376 (Fig 5B).

425 Expression of genes involved in metabolism of nitrogen and sulfur-containing com-
426 pounds were also impacted by human decomposition. Specifically, four of the top
427 ten genes whose expression decreased at day 12 were related to taurine metabolism,
428 with their annotations associated with *tauD*, encoding taurine dioxygenase. (Supple-
429 mentary Table 3). Further investigation into *tauD* showed that mean expression of
430 these genes decreased steadily over one year, beginning at day 12 (Fig 6B); however,
431 *tauD* expression in response to human decomposition was variable across taxonomic
432 associations. Most *tauD* transcripts were associated with *Gammaproteobacteria*, *Acti-*
433 *nobacteria*, *Betaproteobacteria*, *Alphaproteobacteria*, and fungi. While a majority of
434 the *tauD* gene queries displayed reduced expression over time, expression of fungal-
435 associated and a few *Betaproteobacteria*-associated *tauD* genes increased at day
436 58 (Supplementary Fig. 4). Sources of taurine in the human body include taurine
437 absorbed from the diet and taurine produced from anaerobic microbial deconjugation
438 of bile salts via bile salt hydrolase (BSH) enzymes [22]. Therefore, we examined tran-
439 scripts encoding BSH enzymes in decomposition soils. Expression of these genes was
440 elevated at days 12, 58, and 86 before converging toward pre-decomposition levels at
441 days 168 and 376 (Fig 6A). Hierarchical liner mixed effects (HLM) models showed
442 that both *tauD* (HLM $F = 7.356$, $p = 0.002$) and BSH ($F = 13.768$, $p < 0.001$) gene
443 expression was significantly different over time (Fig 6A,B).

Discussion

The goal of this study was to assess microbial gene expression in soils responding to human decomposition. Metatranscriptomics were applied to soil samples collected over one year from below three decomposing human bodies. From this, we found that microbial gene expression reproducibly shifted over time. Additionally, we showed that gene expression profiles had not recovered to pre-decomposition conditions after one year. Comparison of control and decomposition expression profiles revealed that heat-shock proteins were elevated in response to decomposition. We also described expression patterns between decomposition timepoints, noting changes in functional gene categories at certain timepoints, in particular with respect to lipid, nitrogen and sulfur metabolism.

Decomposition impacted soil community gene expression for at least one year

Gene expression profiles remained altered after one year of decomposition. It is unclear if soil microbial communities, in terms of gene expression profiles, had reached a new steady state as a result of decomposition, or if they would eventually return to pre-decomposition conditions. The soil pH, EC, NH_4^+ , NO_3^- , and total nitrogen (TN) exhibited differences (although not statistically significant) in these soils following a year of decomposition, however bacterial and fungal community structures, as assessed by rRNA amplicon libraries, were still altered [13]. This indicates that decomposition can continue to structure microbial communities and impact their function for extended periods of time. While nutrient pools and communities both demonstrate less rapid change at later time points in the study, there is no evidence suggesting an arrival at a steady-state post-disturbance microbial community within our study. In some studies, human decomposition can result in elevated carbon and nutrients (organic nitrogen, ammonium, nitrate, and phosphate) for longer than a year [3], suggesting

decomposition events have long-lasting effects on the local ecosystem. Together, this has implications for terrestrial ecosystem processing (*e.g.*, nutrient cycling, emission of greenhouse gasses, etc.), as we show that decomposition alters functional metabolism pathways within soil microbial communities. It is clear that extended sample collections beyond a single year are needed to address how long microbial communities are affected, and whether there is a return to the original state or some new altered community condition.

Bacteria, fungi, and archaea were all represented by expressed genes throughout decomposition, suggesting that members of all three domains have the potential to contribute to decomposition processes and nutrient cycling. While a majority of annotated transcripts were identified as bacterial, fungal transcripts were the second most abundant group. Fungal transcripts made up almost half (*e.g.*, seven of the top fifteen) of the significantly differentially expressed genes associated with decomposition-impacted soils. Additionally, with respect to expression shifts between decomposition timepoints, fungal transcripts were among the topmost upregulated genes at study day 86. This is not surprising as fungi are key decomposers, involved in the degradation of organic matter in terrestrial ecosystems [23]. It was interesting to see an increase in certain fungal transcripts, such as lipase, at study days 58 and 86 when soil oxygen began to recover. We would expect lipids to enter the soil as tissues are broken down during decomposition, so we were surprised to see bacterial lipase genes decrease during decomposition. This suggests that microbial activity in decomposition soils may be constrained by the changing chemical environment, potentially altered oxygen levels in the case of bacterial lipase gene expression. Prior work with these same soils showed that soil oxygen concentration was a key driver of changes in both bacterial and fungal community composition [13].

Increased stress response during decomposition	553
	554
Soil microbial communities expressed stress response genes in response to human	555
decomposition. Differential expression analysis identified increased expression of mul-	556
multiple heat shock proteins associated with the taxa <i>Xanthomonadales</i> , <i>Actinobacteria</i> ,	557
and fungi. Upon further investigation, expression of these genes increased through day	558
58 and remained high for the remainder of the year. Soil temperature was elevated rel-	559
ative to controls between study days 8 and 80, with maximum temperatures $>40^{\circ}\text{C}$,	560
while soil electrical conductivity increased up to $663\ \mu\text{S cm}^{-1}$ (16X higher than back-	561
ground) through day 58 before slowly decreasing through the remainder of the study.	562
Soil electrical conductivity correlates with ionic strength and can be an indicator	563
of increased salinity [24]. During vertebrate decomposition, elevated conductivity in	564
impacted soils is attributable to sodium (Na), potassium (K), and ammonium (NH_4)	565
[8–11, 13]. As a result, we would expect these microbes to be experiencing both heat	566
and osmotic stress during this period. Prior work has observed increased heat shock	567
gene expression during salt stress in paddy soils [25] and the presence of both heat	568
and osmotic stress genes in desert soils along a salt gradient [26], suggesting saline	569
conditions can alter the expression of heat and/or osmotic stress genes. In our study	570
we observed the stress response within soil microbial communities was stimulated dur-	571
ing human decomposition. At this time, however, it is unclear if expression of these	572
genes is in response to heat stress alone, or in combination with osmotic stress.	573
	574
	575
	576
Increased expression of fungal lipase genes during	577
decomposition	578
	579
	580
	581
Human fat tissue contains lipids that are broken down during decomposition. There-	582
fore, we assessed expression of triacylglycerol lipase genes in decomposition soils. Our	583
results show that expression of triacylglycerol lipase genes was altered in response	584
to decomposition, and these shifts differed between bacterial and fungal transcripts.	585
	586
	587
	588
	589
	590
	591
	592
	593
	594
	595
	596
	597
	598

Specifically, bacterial triacylglycerol lipase transcripts decreased in response to decomposition, while fungal triacylglycerol lipase transcripts increased. Further, expression of these genes corresponded to changes in relative abundance of the fungal classes *Saccharomycetes*, *Sordariomycetes*, and *Eurotiomycetes* [13]. These fungi have been previously associated with decomposition soils [27, 28] and are known to contain triacylglycerol lipase genes in their genomes [29, 30], suggesting that they play a role in lipid degradation in decomposition soils.

Our observation of an overall decrease in triacylglycerol lipase transcripts contrasts with previous work by Howard et al. (2010) [19], who observed increased copies of Group 1 lipase genes via qPCR during swine (*Sus scrofa*) decomposition. Fatty acid composition differs between human and pig tissue [31], potentially altering the lipid profile available for microbes, leading to differences in decomposition products within the soil [18]. These products can then directly or indirectly alter community composition and/or activity of functional proteins via substrate availability or the chemical environment. Further, in a side-by-side comparison of human and pig decomposition at the same location, soil pH increased under pigs, but decreased under humans [18]. Altered pH and soil chemistry could result in different functions and gene expression in decomposition-impacted soils. Many triacylglycerol lipases have a pH optimum that is neutral to basic [32–34], so cells may be decreasing expression under acidic conditions in human decomposition soils. Availability of lipid species and changes to pH may select for taxa that favor these substrates/pH conditions; for example, Mason et al. (2022) [12] showed a relationship between the abundance of the fungal taxa *Saccharomycetes* and antemortem body mass index (BMI) due to relative proportions of fat and muscle tissue.

Evidence for phased denitrification and nitrification

The human body is a concentrated source of nitrogen that is released into the surrounding soil during decomposition. Expression of common marker genes for nitrogen cycling was altered in decomposition soil and suggested nitrogen transformations during human decomposition are driven by soil oxygen concentrations with hydroxylamine as an important intermediate. We observed low or reduced expression of the nitrification genes *nrrA* and *amoA* between days 12 and 86, during a period when oxygen was reduced to 39% - 85%. This was concomitant with an accumulation of ammonium, which reached a maximum on day 12, and low nitrate indicating that nitrification was inhibited. This period of reduced soil oxygen constraining nitrification was also described in a decomposition experiment with beaver (*Castor canadensis*) carcasses Keenan et al. (2018) [8].

We observed increased gene expression for the enzyme hydroxylamine dehydrogenase (HAO) at day 86 while oxygen was reduced (~85%). This corresponded to simultaneous increases in expression of genes encoding subunits of nitric oxide reductase (*norB*) and nitrous oxide reductase (*nosZ*). Traditionally HAO has been thought to process hydroxylamine to nitrite during nitrification, while nitric oxide reductase and nitrous oxide reductase are enzymes involved in the last two steps of denitrification converting nitric oxide (NO) to dinitrogen gas (N₂). However, recent work suggested hydroxylamine can be converted to nitric oxide (NO), and can interact with multiple phases of the nitrogen cycle [35]. Even though *amoA* expression was shown to decrease during reduced oxygen conditions, *amoA* transcripts were still present and likely able to convert ammonium to hydroxylamine as soil oxygen was not completely depleted during decomposition. Additionally, a previous study reported that the growth of the ammonia oxidizing bacteria *Nitrosomonas europaea* under anoxic conditions lead to accumulation of hydroxylamine in a chemostat bioreactor [36], suggesting anaerobic

ammonium oxidation (anammox) may also be occurring in decomposition soils. However, we did not observe increases in *nirK* expression, which might suggest conversion of nitrite to NO for use in the anammox pathway. NO produced via HAO activity may be used for anammox in these soils; however, the role of hydroxylamine as an intermediate in anammox is still debated [35]. Therefore, our current hypothesis is that hydroxylamine accumulates under anaerobic conditions during decomposition, which can then be converted to NO by HAO. This NO would then be present for anaerobic denitrifying bacteria to convert to nitrous oxide (N₂O) by nitric oxide reductase and finally to N₂ by nitrous oxide reductase. Keenan et al. (2018) [8] noted a brief increase in N₂O emissions during beaver carcass decomposition, which suggests denitrification was occurring during this phase of reduced soil oxygen concentrations.

As soils fully reoxygenated by day 168, we observed increased expression of genes encoding enzymes involved in aerobic nitrification, *amoA* and *nxrR*. Nitrification is an oxygen-dependent process which would convert accumulated ammonium to nitrate; the increase in nitrate concentrations may then serve as a substrate for denitrification. We observed increased expression of marker genes encoding all four enzymes in the complete dissimilatory denitrification pathway (*narG*, *nirK*, *norB*, and *nosZ*) at day 376. Increased expression of nitrification and denitrification marker genes is consistent with the accumulation of nitrite, nitrate, and N₂O after oxygen is reintroduced to soils described in Keenan et al. (2018) [3, 8]. Together, gene expression patterns in our study provide further insight into nitrogen transformations in during vertebrate decomposition, suggesting an important role of hydroxylamine.

Increased expression of bile salt hydrolases

Sulfur is present in various organic molecules, including taurine, a sulfur- and nitrogen-rich compound involved in bile acid formation [22]. Taurine in the human body can be absorbed from the diet or synthesized in the liver [37]. However, taurine is also

produced as a byproduct of the deconjugation of bile salts via bile salt hydrolases (BSHs) present in the anaerobic gut taxa *Lactobacillus* and *Clostridium* [22]. We observed increased expression of genes encoding BSH enzymes between days 12 and 86. Given that increased expression of BSH genes corresponded to the beginning of active decomposition, when decomposition products were observed to enter the soil, and the period of reduced dissolved oxygen in our study, it is likely that taurine accumulation is the result of BSH enzyme activity by anaerobic microorganisms. While we did not measure taurine concentrations in the present study, our results correspond to previous decomposition studies that report accumulation of taurine in various organs and body regions [38–40] and soils [18, 41] during decomposition via metabolomics, and increased relative abundance of *Clostridium* and *Lactobacillus* within the body [42–44] and in decomposition soils [20] via DNA sequencing methods, including in these soils [13].

Taurine can be metabolised through desulfurization via the α -ketoglutarate-dependent enzyme taurine dioxygenase (TauD). Specifically, this enzyme, encoded by the gene *tauD*, converts 2-oxoglutarate and taurine to produce aminoacetaldehyde, succinate, sulfite, and CO₂ [45]. Succinate and sulfite from this reaction can then be used for the citric acid cycle and sulfur metabolism, respectively. Given increased BSH expression in our study and reported taurine accumulation in others, we would expect taurine to be present for microbial metabolism by TauD. However, we observed a general decrease in *tauD* expression between days 12 through 376. This trend was driven by reduced expression of *tauD* transcripts associated with *Proteobacteria*, *Gammaproteobacteria*, and *Actinobacteria* whose relative abundance have been shown to remain consistent or increase during human decomposition [20], suggesting that *tauD* expression is downregulated under decomposition conditions. However, we noted that expression of *tauD* genes associated with fungi and a few *Betaproteobacteria* displayed increased representation at day 58, corresponding to increased expression of

783 bile salt hydrolases (BSH) between days 12 and 86. The reduction in *tauD* expres-
784 sion may be due to increased sulfur availability. We did not measure sulfur species
785 in this experiment; however, others have observed increased sulfur concentrations in
786 decomposition-impacted soils [3, 7, 11]. Thus, sulfur scavenging pathways such as tau-
787 rine desulfurization by TauD [46], whose genes are expressed under sulfur-limiting
788 conditions, likely display reduced expression under sulfur replete conditions. Addition-
789 ally, taurine may be processed through other pathways. For example, taurine can be
790 deaminated by taurine dehydrogenase to produce sulfite and acetyl-CoA for carbon
791 metabolism [45, 47]. Overall, our results suggest that human decomposition has poten-
792 tial impacts on soil sulfur biogeochemistry through deposition of inorganic (sulfate)
793 and organic (sulfur-containing amino acids) sulfur compounds.
794
795
796
797
798
799
800
801

802 Conclusion

803

804
805 This study investigated soil microbial gene expression during human decomposition.
806 Metatranscriptomic analysis of soils from three human individuals shows that decom-
807 position impacted microbial community gene expression profiles, exhibiting functional
808 shifts over one year. This included altered expression of genes involved in lipid, N
809 and S metabolism as microbes processed the nutrient-rich tissues of the human body.
810 Additionally, we noted that functionality within decomposition-impacted soils was
811 still affected after one year and had not returned to starting or background condi-
812 tions. Together, these results show that vertebrate decomposition has lasting impacts
813 on local soil ecosystems, including soil microbial communities. These results have
814 important implications for understanding biogeochemical changes due to vertebrate
815 mortality events in terrestrial ecosystems.
816
817
818
819
820
821
822
823
824
825
826
827
828

Materials and Methods

Study design

In February 2018, three deceased male human subjects (hereafter, “donors”) were placed supine on the soil surface at the University of Tennessee Anthropology Research Facility (ARF) and allowed to decompose. Located in Knoxville, TN (35° 56’ 28” N, 83° 56’ 25” W) the ARF is a roughly 2-acre outdoor facility dedicated to studying human decomposition [48]. The soils at the ARF are comprised of the Loyston-Talbott-Rock outcrop (LtD) and Coghill-Corryton (CcD) complexes. LtD soils are a silty clay loam and channery clay overlaying lithic bedrock, while CcD soils are comprised of clay from weathered quartz limestone [13, 48]. A site that had not been previously exposed to decomposition was used for this study.

The decomposition field experiment is fully described in Taylor et al. (2024) [13]. Briefly, experiments were conducted in a block design, where each block consisted of one decomposition site and one control site [13]. In total three blocks, *i.e.*, three donors paired with three respective control sites, were included in the study. Each control site was chosen in a manner to ensure their location was uphill and roughly 2 m away from decomposition sites [13]. Donor internal temperatures were recorded by probes located in the abdomen, while ambient air temperatures were monitored via sensors located roughly 50 cm above the soil surface. Soil temperature and salinity were measured with sensors placed directly underneath each individual (Decagon Devices, GS3) [13]. Donors ranged from 65 to 86 in age and were within 1 kg of each other with regard to weight (90.7 to 91.6 kg); donor BMI varied between 27.7 to 29.6 [13].

875 Sampling and physiochemistry

876
877 Decomposition of all subjects was observed for one year. During the one-year study
878
879 period, soils were sampled at 20 timepoints chosen to correspond with morpho-
880
881 logical stages of decomposition as described by Payne (1965) [49]. Once advanced
882 decay was reached, soils were collected at intervals of 350 accumulated degree days
883
884 (ADD), calculated using ambient air temperatures, up to one year. All soil cores
885
886 were taken using a 1.9 cm (3/4 inch) diameter soil auger to a depth of 16 cm. Soils
887
888 were divided into two depth fractions: 0-1 cm (interface) and 1-16 cm (core) for the
889 analyses reported in Taylor et al. (2024) [13]; the entire 0 to 16 cm core was used
890
891 for this current study. Decomposition soils were taken from directly beneath the
892
893 cadavers, taking care to not re-sample the same location more than once. At the
894
895 time of sampling, soil dissolved oxygen was measured in triplicate using an Orion
896
897 Star™ A329 pH/ISE/Conductivity/Dissolved Oxygen portable multiparameter meter
(ThermoFisher) [13].

898
899
900 A subset of 6 study timepoints were chosen for metatranscriptomics analysis. Study
901
902 days 0, 12, 58, 86, 168, and 376 were chosen as they represented distinct biogeochemi-
903
904 cal phases during decomposition (Supplementary Fig. 5). Study day 0 was chosen as a
905
906 baseline sample prior to cadaver placement. Study day 12 was the start of active decom-
907
908 position, during the initial bloom when soil microbial activity was rapidly increasing
909
910 resulting in the onset of hypoxia: soil ammonium reached maximum concentrations
911
912 and soil oxygen was at minimum (approximately 39%). Study day 58 was during a
913
914 climax period of sustained elevated microbial activity, characterized by high ammo-
915
916 nium concentrations, hypoxia, maximum soil temperatures and minimum soil pH [13].
917
918 Study day 86 represented a period of declining microbial activity, declining hypoxia,
919
920 and increasing nitrate concentrations. Study day 168 was chosen as nitrate was at its
maximum and soil dissolved oxygen had recovered to 99%. Finally, day 376 was cho-
sen to represent the end of the study, 1 year since cadaver placement. Each study day

was represented by four soil samples for RNA extraction: one pooled control sample which was a mix of the three control locations, plus one sample from each of the three donors, yielding a total of 24 samples for this study.

Soil samples were transported to the University of Tennessee (Knoxville, TN) and processed within 24 hours of collection. Soils were homogenized by hand to remove insect larvae, roots, rocks, and other debris (> 2 mm). A subset of soils were used to measure pH, electrical conductivity (EC), and evolved CO_2 as described in Taylor (2024). Soil nitrogen species (NH_4^+ , NO_3^-) and total carbon (TC) and nitrogen (TN) were measured in all soil samples as described in [13]. Reported values for soil physiochemistry represent the full 16 cm core; estimated by summing interface and core values reported by Taylor et. al, (2024) [13] in 1:16 and 15:16 ratios, respectively. Control values reported here are means of the three experimental controls that were unimpacted by decomposition.

Roughly 10 g of soil was reserved for nucleic acid extraction, placed in a 4 oz. Whirl-Pak™ bag (Nasco), flash frozen in liquid nitrogen, and stored at -80°C until further analysis. Bacterial and fungal community composition was assessed via amplicon sequencing of the 16S rRNA gene and ITS2 region as described in Taylor et al. (2024).

RNA Extraction and Sequencing

RNA was extracted from 2 g of soil using Qiagen's RNeasy® PowerSoil® Total RNA kit. Manufacturer's instructions were followed with a few modifications. Soils became saline during decomposition; therefore, we followed the manufacturer's suggestion and incubated all extracts at -20°C following addition of solution SR4 (step 9) to decrease salt precipitation. All RNA samples were resuspended in 40 μl of Solution SR7. RNA concentrations were assessed fluorometrically using the Qubit® RNA HS assay (catalog no. Q32852) with 1 μl of RNA. DNA contamination was removed by DNase

967 treating RNA extracts twice using Qiagen’s DNase Max® kit in 50 µl reactions. RNA
968 concentrations were remeasured after DNase treatment. PCR with V4 16S rRNA gene
969 primers [50, 51] was conducted using RNA extracts as the template to confirm removal
970 of all DNA prior to sequencing. RNA aliquots were shipped to HudsonAlpha Dis-
971 covery (Huntsville, AL) for library preparation and RNA sequencing. Dual-indexed
972 libraries were prepared using the Illumina® Stranded Total RNA prep with riboso-
973 mal RNA depletion via ligation with Ribo-Zero Plus. Libraries were then pooled and
974 sequenced on Illumina’s NovaSeq 6000 v4 platform, resulting in demultiplexed fastq
975 files for each sample.
976
977
978
979
980
981
982

983 Bioinformatics

984
985 Illumina sequencing of the 24 libraries yielded a total of 5,073,476,730 reads, or
986 2,536,738,365 paired reads, with a mean of 105,697,432 paired reads per sample. Read
987 quality control (QC) was conducted in KBase [52] using Trimmomatic [53]. Paired
988 fastq files were imported to KBase through Globus. Poor quality reads were removed
989 (4.7% of all reads), and adapters trimmed via Trimmomatic (v0.36) using default set-
990 tings and the TruSeq3-PE-2 adapter file, resulting in 4,834,123,062 total reads. After
991 QC check with FastQC, trimmed libraries were exported as fastq files from KBase
992 through Globus. Remaining ribosomal RNA was filtered using bbmap (maxindel =
993 20, minid = 0.93) from the Joint Genome Institute’s (JGI) bbtools suite [54]. Fil-
994 tering of ribosomal RNA further removed 7.3% of reads, leaving 4,479,804,360 reads
995 for assembly. Following this step, all non-ribosomal reads from all 24 samples were
996 merged into one file. Reads were then co-assembled into contigs using the de novo
997 assembler MEGAHIT (v1.2.9) [55] (-12 -k-min 23, -k-max 123, -k-step 10).
998
999
1000
1001
1002
1003
1004
1005
1006
1007
1008 Gene identification and annotation from co-assembled contigs was performed using
1009 Prodigal [56] and eggNOG mapper [57], respectively. Briefly, the DNA fasta contain-
1010 ing all contigs was submitted to Prodigal (v2.6.3) for protein coding gene predication
1011
1012

for a meta-sample (-p meta -f gff). After co-assembly, a total of 6,257,674 gene calls were identified by Prodigal. Next, predicated genes were functionally and taxonomically annotated using eggNOG mapper (v2.1.6) using basic settings to perform a diamond blastp search [58]. From this, 1,048,573 proteins were annotated by eggNOG-mapper (16.7%). Most of the annotated proteins were taxonomically annotated as bacteria (91.3%), followed by eukaryotes (7.6 %), and archaea (0.81 %). Of the 7.6% of eukaryotic proteins, 64.4% (4.9% of all proteins) were annotated as fungi. For this study, genes of interest included all bacterial, archaeal, and fungal proteins, therefore all non-fungal eukaryotic proteins (32,004) were removed prior to downstream analysis. Transcript counts for all genes of interest were obtained by mapping reads from each respective sample to genes of interest obtained from co-assembly using QIAGEN CLC Genomics Workbench 20.0 (<https://digitalinsights.qiagen.com/>). The percent of reads mapped to genes of interest ranged from 21% to 38% between samples, with an average of 31% reads mapped. Gene counts were then combined in a single file and used for downstream analyses in R.

Differential Expression

Transcript counts from all samples were combined in a single workable data file and imported into R for differential expression analysis using the R packages edgeR [59] and limma [60] following a modified pipeline by Phipson et al. (2020) [61]. The transcript count table was imported into R and converted to a DGElist object. Genes without sufficient counts for statistical analysis were removed to increase power using the edgeR function filterByExpr(), using study day as the comparison group.

Raw counts were then log2 normalized and gene expression profiles compared via multidimensional scaling (MDS) and hierarchical clustering. Multidimensional scaling (MDS) was conducted using plotMDS() from the limma package to assess differences between samples. MDS values were extracted from the MDS object, and the first two

1059 dimensions plotted using ggplot2 [62]. We also assessed the relationship between gene
 1060 expression profiles and changes in the soil environment using canonical correspondence
 1061 analysis (CCA). Environmental variables of interest included decomposition time in
 1062 accumulated degree hours (ADH) based on ambient temperatures, ADH based on
 1063 internal gut temperatures, ADH based on soil temperatures, gravimetric moisture,
 1064 pH, electrical conductivity (EC), dissolved oxygen (DO), CO₂ (μmol gdw⁻¹), NH₄ (mg
 1065 gdw⁻¹), NO₃ (mg gdw⁻¹), N %, C %, and CN ratio. First, permutational multivariate
 1066 analysis of variance (PERMANOVA) with adonis() (vegan v2.6.7) [63] was used to
 1067 identify significant soil parameters. Then the vegan functions cca() and scores() were
 1068 applied to run the CCA and extract scores, respectively. Scores for the first two
 1069 dimension were plotted using ggplot2, with loadings extracted from the CCA biplot.
 1070 For differential expression analysis, raw filtered reads were normalized using edgeR's
 1071 trimmed mean of M values (TMM) normalization using the function calcNormFac-
 1072 tors(). TMM normalized reads were then log2 transformed using limma's voom() and
 1073 differential expression assessed. Empirical Bayes shrinkage was used correct to p-
 1074 values for false discovery rates. The topmost up and down regulated genes for each
 1075 comparison, determined by log2 fold change and adjusted p-values, were then reported.
 1076 Expression of certain genes were assessed after performing transcripts per million
 1077 (TPM) normalization and statistical analyses with a combination of analysis of vari-
 1078 ance (ANOVA) and post-hoc Tukey tests. ANOVA across all timepoints were applied
 1079 to hierarchical linear mixed effects models to account for repeated sampling within
 1080 each donor block.

1098 Data availability

1099 Raw RNA sequence files from the Illumina Novaseq are available at the National Cen-
 1100 ter for Biotechnology Information's (NCBI) Sequence Read Archive (SRA) as a part
 1101
 1102
 1103
 1104

of [BioProject PRJNA1066312](#) under BioSample accession numbers SAMN45195141-
SAMN45195164. Additional datasets supporting the conclusions of this article are
available on [GitHub](#).

Code availability

The code used for analysis and to generate figures are available on [GitHub](#).

References

- [1] Benninger, L. A., Carter, D. O. & Forbes, S. L. The biochemical alteration of soil
beneath a decomposing carcass. *Forensic Science International* **180**, 70–5 (2008).
- [2] Towne, E. G. Prairie vegetation and soil nutrient responses to ungulate carcasses.
Oecologia **122**, 232–239 (2000). URL <https://doi.org/10.1007/PL00008851>.
- [3] DeBruyn, J. M., Keenan, S. W. & Taylor, L. S. From carrion to soil: microbial
recycling of animal carcasses. *Trends in Microbiology* (2024). URL <https://doi.org/10.1016/j.tim.2024.09.003>. Publisher: Elsevier.
- [4] Parmenter, R. R. & MacMahon, J. A. Carrion decomposition and nutrient cycling
in a semiarid shrub–steppe ecosystem. *Ecological Monographs* **79**, 637–661 (2009).
- [5] Macdonald, B. C. T. *et al.* Carrion decomposition causes large and lasting effects
on soil amino acid and peptide flux. *Soil Biology and Biochemistry* **69**, 132–140
(2014).
- [6] Bump, J. K. *et al.* Ungulate carcasses perforate ecological filters and create
biogeochemical hotspots in forest herbaceous layers allowing trees a competitive
advantage. *Ecosystems* **12**, 996–1007 (2009).

- 1151 [7] Aitkenhead-Peterson, J. A., Owings, C. G., Alexander, M. B., Larison, N. &
1152 Bytheway, J. A. Mapping the lateral extent of human cadaver decomposition
1153 with soil chemistry. *Forensic Science International* **216**, 127–34 (2012).
1154
1155
1156
1157 [8] Keenan, S. W., Schaeffer, S. M., Jin, V. L. & DeBruyn, J. M. Mortality hotspots:
1158 nitrogen cycling in forest soils during vertebrate decomposition. *Soil Biology and*
1159 *Biochemistry* **121**, 165–176 (2018).
1160
1161
1162
1163 [9] Fancher, J. P. *et al.* An evaluation of soil chemistry in human cadaver decom-
1164 position islands: Potential for estimating postmortem interval (PMI). *Forensic*
1165 *Science International* **279**, 130–139 (2017).
1166
1167
1168
1169 [10] Quaggiotto, M.-M., Evans, M. J., Higgins, A., Strong, C. & Barton, P. S.
1170 Dynamic soil nutrient and moisture changes under decomposing vertebrate
1171 carcasses. *Biogeochemistry* **146**, 71–82 (2019).
1172
1173
1174 [11] Taylor, L. S. *et al.* Soil elemental changes during human decomposition.
1175 *PLoS ONE* **18**, 1–24 (2023). URL <https://doi.org/10.1371/journal.pone.0287094>.
1176
1177 Publisher: Public Library of Science.
1178
1179
1180 [12] Mason, A. R. *et al.* Body mass index (BMI) impacts soil chemical and microbial
1181 response to human decomposition. *mSphere* e0032522 (2022).
1182
1183
1184 [13] Taylor, L. S. *et al.* Transient hypoxia drives soil microbial community dynamics
1185 and biogeochemistry during human decomposition. *FEMS Microbiology Ecology*
1186 **100**, fae119 (2024). URL <https://doi.org/10.1093/femsec/fae119>.
1187
1188
1189
1190 [14] Keenan, S. W., Emmons, A. L. & DeBruyn, J. M. Microbial community coa-
1191 lesence and nitrogen cycling in simulated mortality decomposition hotspots.
1192 *Ecological Processes* **12**, 45 (2023). URL [https://doi.org/10.1186/s13717-023-](https://doi.org/10.1186/s13717-023-00451-y)
1193
1194
1195
1196

- [15] Mason, A. R., Taylor, L. S. & DeBruyn, J. M. Microbial ecology of vertebrate decomposition in terrestrial ecosystems. *FEMS Microbiology Ecology* **99**, fiad006 (2023). URL <https://doi.org/10.1093/femsec/fiad006>.
- [16] Burcham, Z. M. *et al.* Total RNA analysis of bacterial community structural and functional shifts throughout vertebrate decomposition. *Journal of Forensic Sciences* **64**, 1707–1719 (2019).
- [17] Ashe, E. C., Comeau, A. M., Zejdlik, K. & O’Connell, S. P. Characterization of bacterial community dynamics of the human mouth throughout decomposition via metagenomic, metatranscriptomic, and culturing techniques. *Frontiers in Microbiology* **12**, 689493 (2021).
- [18] DeBruyn, J. M. *et al.* Comparative decomposition of humans and pigs: soil biogeochemistry, microbial activity and metabolomic profiles. *Frontiers in Microbiology* **11**, 608856 (2021).
- [19] Howard, G. T., Duos, B. & Watson-Horzelski, E. J. Characterization of the soil microbial community associated with the decomposition of a swine carcass. *International Biodeterioration & Biodegradation* **64**, 300–304 (2010).
- [20] Cobaugh, K. L., Schaeffer, S. M. & DeBruyn, J. M. Functional and structural succession of soil microbial communities below decomposing human cadavers. *Plos One* **10**, e0130201 (2015).
- [21] Singh, B. *et al.* Temporal and spatial impact of human cadaver decomposition on soil bacterial and arthropod community structure and function. *Frontiers in Microbiology* **8**, 2616 (2018).
- [22] Urdaneta, V. & Casadesús, J. Interactions between bacteria and bile salts in the gastrointestinal and hepatobiliary tracts. *Frontiers in Medicine* **4** (2017).

1243 [23] van der Wal, A., Geydan, T. D., Kuyper, T. W. & de Boer, W. A thready affair:
1244 linking fungal diversity and community dynamics to terrestrial decomposition
1245 processes. *FEMS Microbiology Reviews* **37**, 477–494 (2013).
1246
1247
1248
1249 [24] Essington, M. E. *Soil and water chemistry: an integrative approach* (CRC press,
1250 2015).
1251
1252
1253 [25] Peng, J., Wegner, C.-E. & Liesack, W. Short-term exposure of paddy soil micro-
1254 bial communities to salt stress triggers different transcriptional responses of key
1255 taxonomic groups. *Frontiers in Microbiology* **8** (2017).
1256
1257
1258
1259 [26] Pandit, A. S. *et al.* A snapshot of microbial communities from the Kutch: one of
1260 the largest salt deserts in the World. *Extremophiles* **19**, 973–987 (2015).
1261
1262
1263 [27] Metcalf, J. L. *et al.* Microbial community assembly and metabolic function during
1264 mammalian corpse decomposition. *Science* **351**, 158–62 (2016).
1265
1266
1267 [28] Fu, X. *et al.* Fungal succession during mammalian cadaver decomposition and
1268 potential forensic implications. *Scientific Reports* **9**, 12907 (2019).
1269
1270
1271 [29] Dujon, B. *et al.* Genome evolution in yeasts. *Nature* **430**, 35–44 (2004).
1272
1273
1274 [30] Haridas, S. *et al.* The genome and transcriptome of the pine saprophyte *Ophios-*
1275 *toma piceae*, and a comparison with the bark beetle-associated pine pathogen
1276 *Grosmannia clavigera*. *BMC Genomics* **14**, 373 (2013).
1277
1278
1279
1280 [31] Notter, S. J., Stuart, B. H., Rowe, R. & Langlois, N. The initial changes of fat
1281 deposits during the decomposition of human and pig remains. *Journal of Forensic*
1282 *Sciences* **54**, 195–201 (2009).
1283
1284
1285 [32] Kok, R. G. *et al.* Characterization of the extracellular lipase, LipA, of *Acineto-*
1286 *bacter calcoaceticus* BD413 and sequence analysis of the cloned structural gene.
1287
1288

	<i>Molecular Microbiology</i> 15 , 803–818 (1995).	1289
		1290
[33]	Hasan, F., Shah, A. A. & Hameed, A. Influence of culture conditions on lipase production by <i>Bacillus</i> sp. FH5. <i>Annals of Microbiology</i> 56 , 247–252 (2006).	1291
		1292
		1293
		1294
		1295
[34]	Zouaoui, B. & Bouziane, A. Production, optimization and characterization of the lipase from <i>Pseudomonas aeruginosa</i> . <i>Romanian Biotechnological Letters</i> 17 , 7187–7193 (2012).	1296
		1297
		1298
		1299
		1300
[35]	Soler-Jofra, A., Pérez, J. & van Loosdrecht, M. C. M. Hydroxylamine and the nitrogen cycle: A review. <i>Water Research</i> 190 , 116723 (2021).	1301
		1302
		1303
		1304
		1305
[36]	Yu, R., Perez-Garcia, O., Lu, H. & Chandran, K. <i>Nitrosomonas europaea</i> adaptation to anoxic-oxic cycling: Insights from transcription analysis, proteomics and metabolic network modeling. <i>Science of the Total Environment</i> 615 , 1566–1573 (2018).	1306
		1307
		1308
		1309
		1310
		1311
		1312
[37]	Seidel, U., Huebbe, P. & Rimbach, G. Taurine: A regulator of cellular redox homeostasis and skeletal muscle function. <i>Molecular Nutrition & Food Research</i> 63 , 1800569 (2019).	1313
		1314
		1315
		1316
		1317
		1318
[38]	Mora-Ortiz, M., Trichard, M., Oregioni, A. & Claus, S. P. Thanatometabolomics: introducing NMR-based metabolomics to identify metabolic biomarkers of the time of death. <i>Metabolomics</i> 15 , 37 (2019).	1319
		1320
		1321
		1322
		1323
		1324
[39]	Locci, E. <i>et al.</i> A ¹ H NMR metabolomic approach for the estimation of the time since death using aqueous humour: an animal model. <i>Metabolomics</i> 15 , 76 (2019).	1325
		1326
		1327
		1328
[40]	Zelentsova, E. A. <i>et al.</i> Post-mortem changes in the metabolomic compositions of rabbit blood, aqueous and vitreous humors. <i>Metabolomics</i> 12 , 172 (2016).	1329
		1330
		1331
		1332
		1333
		1334

1335 [41] Hoeland, K. M. *Investigating the potential of postmortem metabolomics in mam-*
1336 *malian decomposition studies in outdoor settings.* Ph.D. thesis, University of
1337 Tennessee-Knoxville, https://trace.tennessee.edu/utk_graddiss/7000 (2021).
1338
1339
1340
1341 [42] Javan, G. T. *et al.* Human thanatobiome succession and time since death.
1342 *Scientific Reports* **6**, 29598 (2016).
1343
1344
1345 [43] Javan, G. T., Finley, S. J., Smith, T., Miller, J. & Wilkinson, J. E. Cadaver
1346 thanatobiome signatures: the ubiquitous nature of Clostridium species in
1347 human decomposition. *Frontiers in Microbiology* **8**, 2096 (2017).
1348
1349
1350
1351 [44] DeBruyn, J. M. & Hauther, K. A. Postmortem succession of gut microbial
1352 communities in deceased human subjects. *Peerj* **5**, e3437 (2017).
1353
1354
1355 [45] Cook, A. M. & Denger, K. *Metabolism of taurine in microorganisms*, 3–13 (2006).
1356
1357
1358 [46] Kertesz, M. A. Riding the sulfur cycle – metabolism of sulfonates and sul-
1359 fate esters in Gram-negative bacteria. *FEMS Microbiology Reviews* **24**, 135–175
1360 (2000).
1361
1362
1363 [47] Enzymes and genes of taurine and isethionate dissimilation in
1364 *Paracoccus denitrificans*, volume = 150, issn = 1465-2080, doi =
1365 <https://doi.org/10.1099/mic.0.26795-0>, abstract = Growth of the -
1366
1367
1368 proteobacterium Paracoccus denitrificans NKNIS with taurine or isethionate as
1369 sole source of carbon involves sulfoacetaldehyde acetyltransferase (Xsc), which
1370 is presumably encoded by an xsc gene in subgroup 3, none of whose gene prod-
1371 ucts has been characterized. The genome of the -proteobacterium Rhodobacter
1372 sphaeroides 2.4.1 was interpreted to contain a nine-gene cluster encoding the
1373 inducible dissimilation of taurine, and this deduced pathway included a regu-
1374
1375
1376
1377
1378
1379
1380

presumably TauXY) as well as Xsc (subgroup 3), a hypothetical protein and
phosphate acetyltransferase (Pta). A similar cluster was found in *P. denitrificans*
NKNIS, in contrast to an analogous cluster encoding an ATP-binding cassette
transporter in *Paracoccus pantotrophus*. Inducible TDH, Xsc and Pta were
found in extracts of taurine-grown cells of strain NKNIS. TDH oxidized taurine
to sulfoacetaldehyde and ammonium ion with cytochrome c as electron acceptor.
Whereas Xsc and Pta were soluble enzymes, TDH was located in the particulate
fraction, where inducible proteins with the expected masses of TauXY (14 and
50 kDa, respectively) were detected by SDS-PAGE. Xsc and Pta were separated
by anion-exchange chromatography. Xsc was effectively pure; the molecular
mass of the subunit (64 kDa) and the N-terminal amino acid sequence confirmed
the identification of the xsc gene. Inducible isethionate dehydrogenase (IDH),
Xsc and Pta were assayed in extracts of isethionate-grown cells of strain NKNIS.
IDH was located in the particulate fraction, oxidized isethionate to sulfoacetalde-
hyde with cytochrome c as electron acceptor and correlated with the expression
of a 62 kDa protein. Strain NKNIS excreted sulfite and sulfate during growth
with a sulfonate and no sulfite dehydrogenase was detected. There is consider-
able biochemical, genetic and regulatory complexity in the degradation of these
simple molecules., number = 4, journal = Microbiology, author = Brüggemann,
Chantal and Denger, Karin and Cook, Alasdair M. and Ruff, Jürgen, year =
2004, keywords = ABC transporter, ATP-binding cassette transporter, DCPIP,
dichlorophenol indophenol, IDH, isethionate dehydrogenase, MALDI-TOF-MS,
matrix-assisted, laser-desorption ionization time-of-flight mass spectrometry,
Pta, phosphate acetyltransferase, TDH, taurine dehydrogenase, ThDP, thiamin
diphosphate, Tpa, taurine:pyruvate aminotransferase, TRAP transporter, tri-
partite ATP-independent transporter, Xsc, sulfoacetaldehyde acetyltransferase,
pages = 805–816, .

1427 [48] Keenan, S. W. *et al.* Spatial impacts of a multi-individual grave on microbial
1428 and microfaunal communities and soil biogeochemistry. *PLoS One* **13**, e0208845
1429 (2018).
1430
1431
1432
1433 [49] Payne, J. A. A summer carrion study of the baby pig *Sus Scrofa* linnaeus. *Ecology*
1434 **46**, 592–602 (1965).
1435
1436
1437 [50] Apprill, A., McNally, S., Parsons, R. & Weber, L. Minor revision to V4 region SSU
1438 rRNA 806R gene primer greatly increases detection of SAR11 bacterioplankton.
1439 *Aquatic Microbial Ecology* **75**, 129–137 (2015).
1440
1441
1442
1443 [51] Parada, A. E., Needham, D. M. & Fuhrman, J. A. Every base matters: assessing
1444 small subunit rRNA primers for marine microbiomes with mock communities,
1445 time series and global field samples. *Environmental Microbiology* **18**, 1403–14
1446 (2016).
1447
1448
1449
1450 [52] Arkin, A. P. *et al.* KBase: The United States Department of Energy Systems
1451 Biology Knowledgebase. *Nature Biotechnology* **36**, 566–569 (2018).
1452
1453
1454 [53] Bolger, A. M., Lohse, M. & Usadel, B. Trimmomatic: a flexible trimmer for
1455 Illumina sequence data. *Bioinformatics* **30**, 2114–2120 (2014).
1456
1457
1458
1459 [54] Bushnell, B. BBTools software package (2014).
1460
1461 [55] Li, D., Liu, C.-M., Luo, R., Sadakane, K. & Lam, T.-W. MEGAHIT: an ultra-fast
1462 single-node solution for large and complex metagenomics assembly via succinct
1463 de Bruijn graph. *Bioinformatics* **31**, 1674–1676 (2015).
1464
1465
1466
1467 [56] Hyatt, D. *et al.* Prodigal: prokaryotic gene recognition and translation initiation
1468 site identification. *BMC Bioinformatics* **11**, 119 (2010).
1469
1470
1471
1472

- [57] Cantalapiedra, C. P., Hernández-Plaza, A., Letunic, I., Bork, P. & Huerta-Cepas, J. eggNOG-mapper v2: functional annotation, orthology assignments, and domain prediction at the metagenomic scale. *Molecular Biology and Evolution* **38**, 5825–5829 (2021).
- [58] Buchfink, B., Reuter, K. & Drost, H.-G. Sensitive protein alignments at tree-of-life scale using DIAMOND. *Nature Methods* **18**, 366–368 (2021).
- [59] Robinson, M. D., McCarthy, D. J. & Smyth, G. K. edgeR: a Bioconductor package for differential expression analysis of digital gene expression data. *Bioinformatics* **26**, 139–140 (2010).
- [60] Smyth, G. K. in *limma: Linear Models for Microarray Data* (eds Gentleman, R., Carey, V. J., Huber, W., Irizarry, R. A. & Dudoit, S.) *Bioinformatics and Computational Biology Solutions Using R and Bioconductor* 397–420 (Springer New York, New York, NY, 2005).
- [61] Phipson, B. *et al.* Differential expression analysis (2020). URL <https://combine-australia.github.io/RNAseq-R/06-rnaseq-day1.html#References>.
- [62] Wickham, H. *ggplot2: Elegant Graphics for Data Analysis* (Springer-Verlag New York, 2016). URL <https://ggplot2.tidyverse.org>.
- [63] Oksanen, J. *et al.* *vegan: Community Ecology Package* (2024). URL <https://vegandevs.github.io/vegan/>.

1519 **Figures**

1520

1521

1522 **Figure 1: Microbial gene expression profiles are altered during human**
1523 **decomposition.** Multidimensional scaling (MDS) shows gene expression within soils
1524 changed as decomposition progressed (A). Canonical correspondence analysis (CCA)
1525 shows that environmental variables explained 47.3% of the variation in gene expres-
1526 sion profiles (B). Variables in bold red type significantly ($p < 0.05$) explained some
1527 of the variation in gene expression profiles as assessed by Permutational Analysis of
1528 Variance (PERMANOVA). In both panels soils from controls (CON) and the three
1529 donors (SP1, SP2, SP3) are denoted by symbol shape, while color represents study
1530 day. In B, soil physiochemical variable loadings are represented by arrows: Gravimetric
1531 water content (GWC), electrical conductivity (EC), pH (pH), dissolved oxygen (DO),
1532 respiration (evolved CO_2 $\mu\text{mol gdw}^{-1}$), ammonium (NH_4), and nitrate (NO_3) concen-
1533 trations (mg gdw^{-1}), percent carbon (%C), percent nitrogen (%N), carbon:nitrogen
1534 ratio (C:N), ambient temperature (T_A), and soil temperature (T_S).

1535

1536

1537

1538

1539

1540

1541

1542

1543

1544

1545

1546

1547

1548

1549

1550

1551

1552

1553

1554

1555

1556

1557

1558

1559

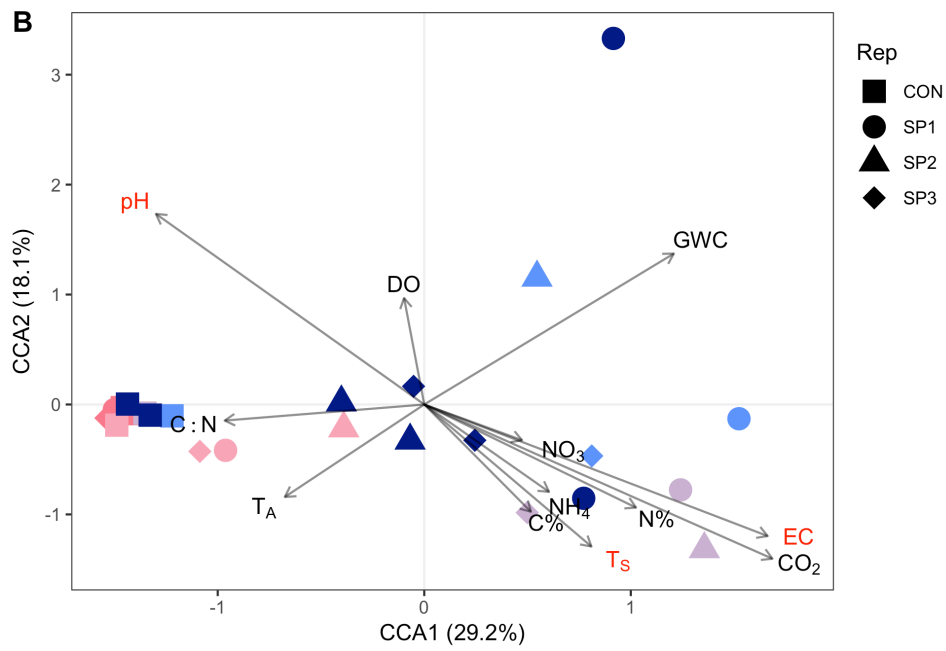
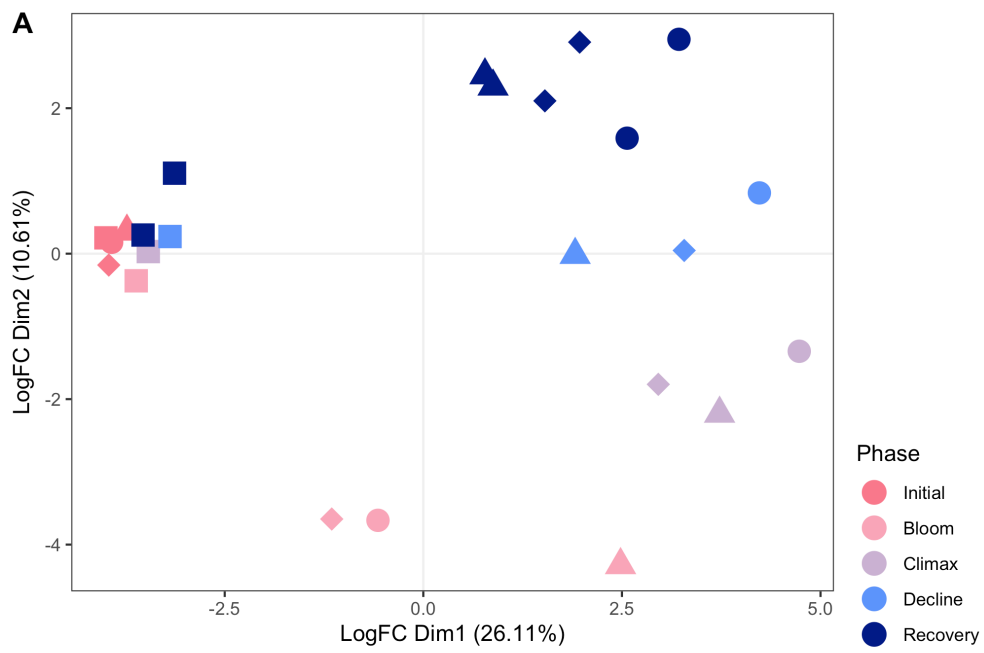
1560

1561

1562

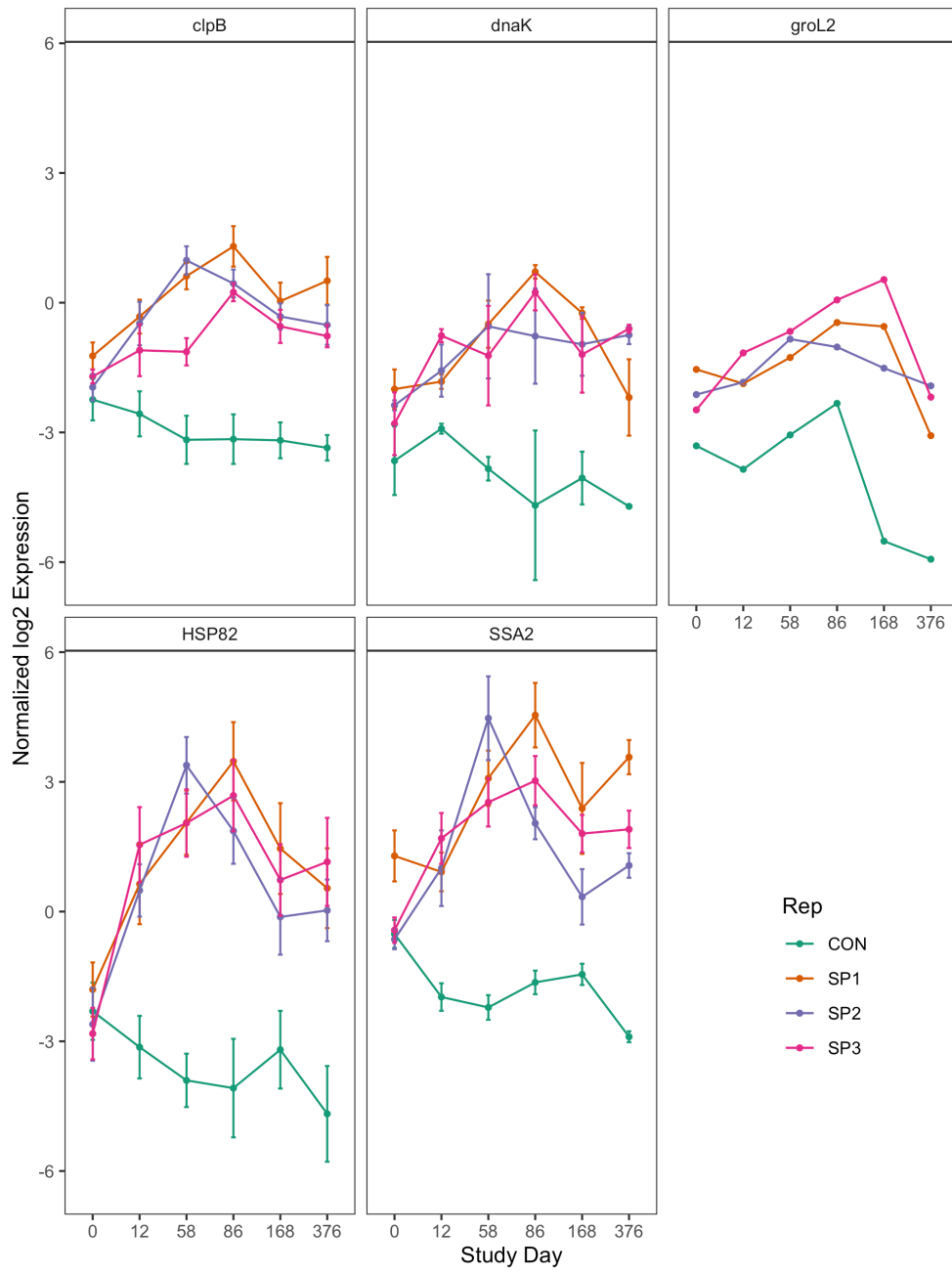
1563

1564



1611 **Figure 2: Mean normalized log2 expression of heat shock proteins identified**
1612 **by differential expression analysis comparing decomposition and control**
1613 **soils.** Each panel represents a single heat shock gene, labeled with gene names, identified via Prodigal. Symbol color denotes if the sample is a control (CON, green), or
1614 one of three individuals: SP1 (orange), SP2 (purple), or SP3 (pink). Error bars are
1615 standard error of individual query genes in the top 20 transcripts associated with
1616 decomposition soils.
1617
1618

1619
1620
1621
1622
1623
1624
1625
1626
1627
1628
1629
1630
1631
1632
1633
1634
1635
1636
1637
1638
1639
1640
1641
1642
1643
1644
1645
1646
1647
1648
1649
1650
1651
1652
1653
1654
1655
1656



1703 **Figure 3: Top twenty up- and down-regulated genes in decomposition soils**
1704 **comparing sequential study days (0, 12, 58, 86, 168, 376) colored by COG**
1705 **functional category (A) and taxonomic annotation (B). Positive values denote**
1706 **increased expression compared to the preceding timepoint, while negative values**
1707 **denote a decrease.**

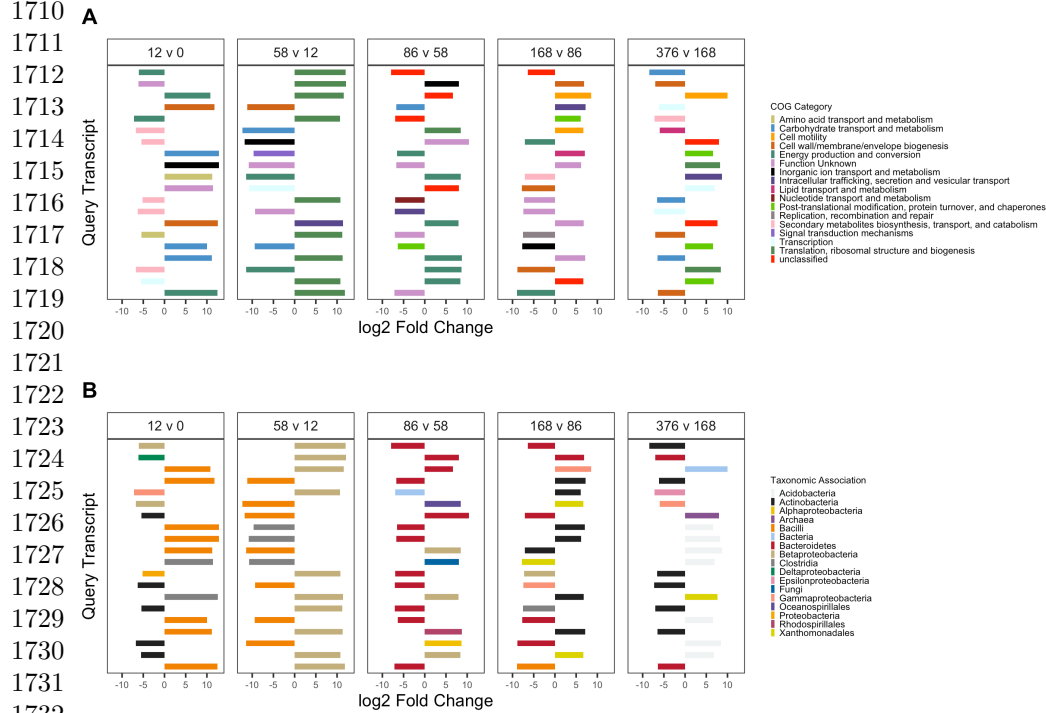
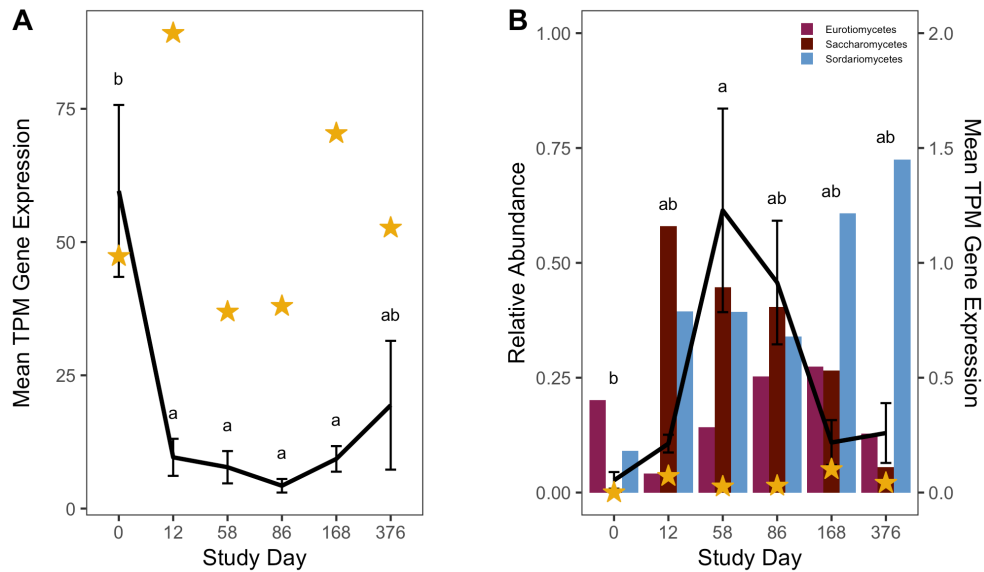


Figure 4: Mean transcript abundance, in transcripts per million (TPM), of all bacterial (A) and fungal (B) triacylglycerol lipase (EC 3.1.1.3) genes over time. Abundance of both bacterial ($p = 0.001$) and fungal ($p = 0.015$) lipase transcripts change significantly over time. Black lines (A, B) report mean and standard deviation of TPM from three individuals (black line), while gold stars denote mean TPM in control soils. Letters are the result of post-hoc Tukey tests between decomposition timepoints. In B, bars show the relative abundance of the fungal classes *Saccharomycetes*, *Sordariomycetes*, and *Eurotiomycetes*, reported in Taylor et al. (2024).



1795 **Figure 5: Mean gene expression, in transcripts per million (TPM), of com-**
1796 **monly used marker genes for enzymes involved in nitrogen cycling over**
1797 **time in controls (A) and decomposition (B) soils. Data in B represent mean**
1798 **and standard deviation of TPM from three individuals.**
1799

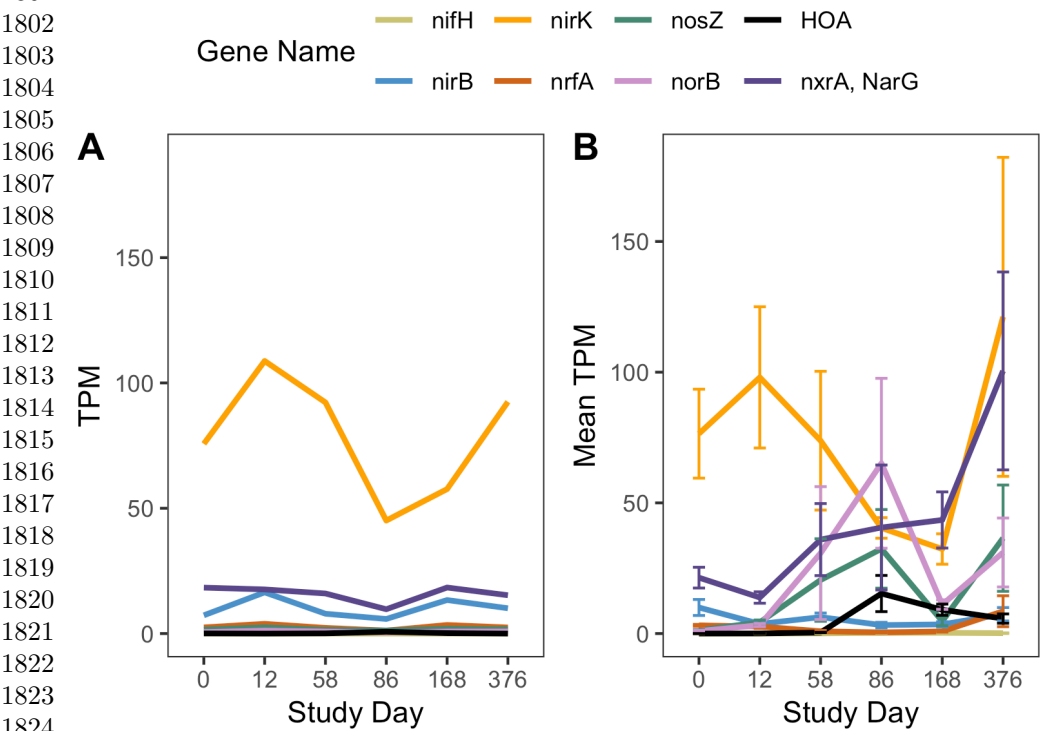
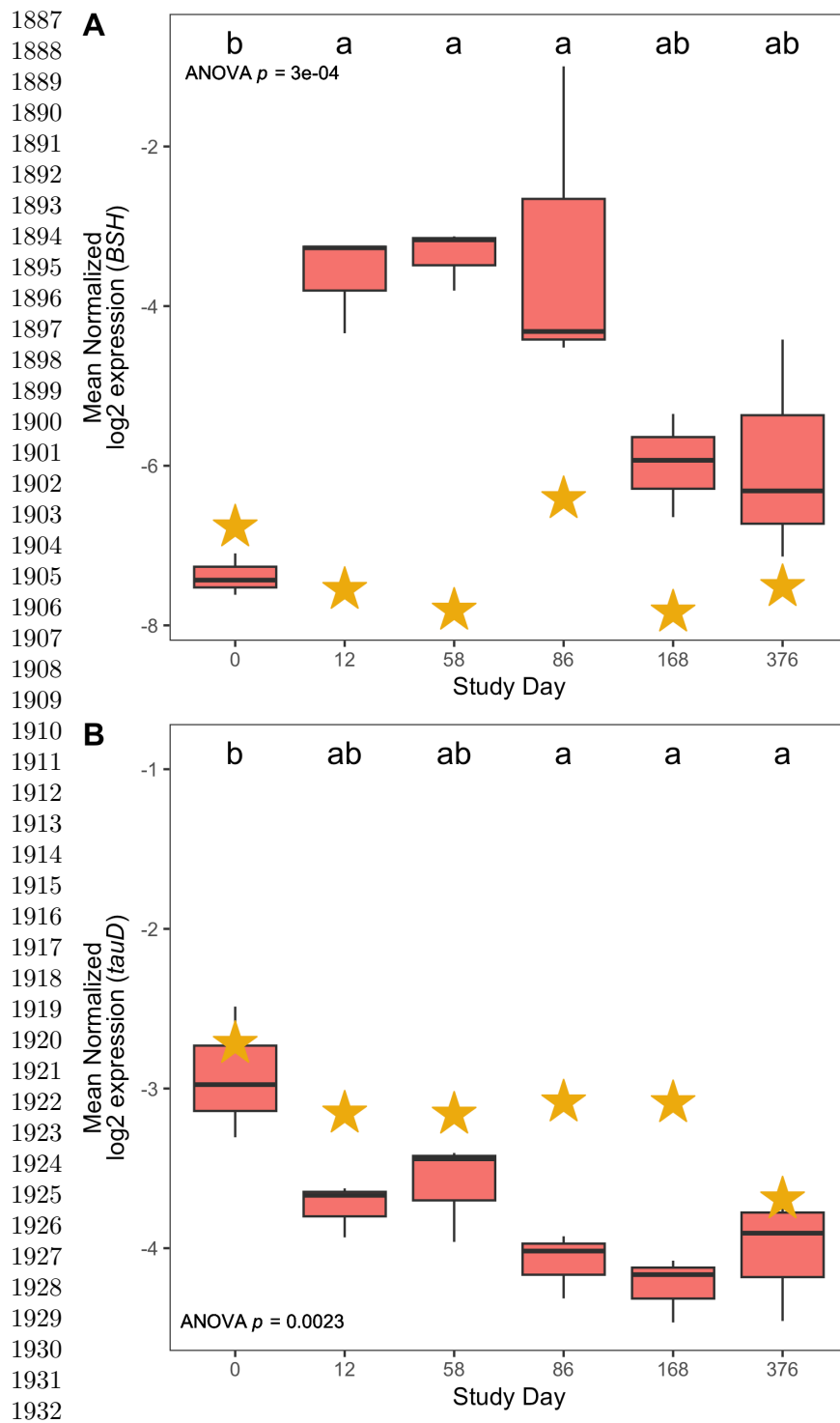


Figure 6: Mean bile salt hydrolase, BSH, (A) and *tauD*, taurine dioxy-
genase, (B) log2 normalized expression in controls (gold stars) and
decomposition (boxplots) soils. Boxplots display the 25th and 75th quartiles
and median log2 normalized values between all three individuals at each timepoint.
ANOVA p-value is the result of a hierarchical linear mixed effects model accounting
for repeated measures of each donor block, while letters denote the results of *post-hoc*
Tukey test.

1841
1842
1843
1844
1845
1846
1847
1848
1849
1850
1851
1852
1853
1854
1855
1856
1857
1858
1859
1860
1861
1862
1863
1864
1865
1866
1867
1868
1869
1870
1871
1872
1873
1874
1875
1876
1877
1878
1879
1880
1881
1882
1883
1884
1885
1886



Acknowledgements

We would like to thank the Forensic Anthropology Center at the University of Tennessee-Knoxville for their help in setting up field experiments. We would like to thank Mary Davis for her help in managing the field site and helping to obtain donors for this work. This research was funded by a National Institute of Justice Award (DOJ-NIJ-2017-R2-CX-0008) to LST and JMD.

1933
1934
1935
1936
1937
1938
1939
1940
1941
1942
1943
1944
1945
1946
1947
1948
1949
1950
1951
1952
1953
1954
1955
1956
1957
1958
1959
1960
1961
1962
1963
1964
1965
1966
1967
1968
1969
1970
1971
1972
1973
1974
1975
1976
1977
1978